Minimal theory of massive gravity in the light of CMB data and the S_8 tension

José C. N. de Araujo,[1,*] Antonio De Felice,[2,†] Suresh Kumar,[3,4,‡] and Rafael C. Nunes[1,§]

[1]*Divisão de Astrofísica, Instituto Nacional de Pesquisas Espaciais, Avenida dos Astronautas 1758, São José dos Campos, 12227-010, São Paulo, Brazil*

[2]*Center for Gravitational Physics, Yukawa Institute for Theoretical Physics, Kyoto University, 606-8502, Kyoto, Japan*

[3]*Department of Mathematics, Indira Gandhi University, Meerpur, Haryana-122502, India*

[4]*Department of Mathematics, BITS Pilani, Pilani Campus, Rajasthan-333031, India*

(Received 17 June 2021; accepted 15 October 2021; published 23 November 2021)

We investigate the minimal theory of massive gravity (MTMG) in the light of different observational datasets that are in tension within the Λ cold dark matter cosmology. In particular, we analyze the MTMG model, for the first time, with the Planck–cosmic microwave background (CMB) data, and how these precise measurements affect the free parameters of the theory. The MTMG model can affect the CMB power spectrum at large angular scales and cause a suppression on the amplitude of the matter power spectrum. We find that on adding Planck-CMB data, the graviton has a small, positive, but nonzero mass at 68% confidence level, and from this perspective, we show that the tension between redshift space distortions measurements and Planck-CMB data in the parametric space $S_8 - \Omega_m$ can be resolved within the MTMG scenario. Through a robust and accurate analysis, we find that the H_0 tension between the CMB and the local distance ladder measurements still remains but can be reduced to $\sim 3.5\sigma$ within the MTMG theory. The MTMG is very well consistent with the CMB observations, and undoubtedly, it can serve as a viable candidate among other modified gravity theories.

DOI: 10.1103/PhysRevD.104.104057

I. INTRODUCTION

Over the past two decades, a large volume of cosmological information has been obtained by several data surveys, making the estimates of cosmological parameters increasingly accurate. The understanding of the cosmological probes has been well modeled through the standard Λ cold dark matter scenario (the ΛCDM scenario). The ΛCDM cosmological model provides a wonderful fit to the current cosmological data, but recently a few tensions and anomalies became statistically significant while analyzing different datasets. The most discussed tension in the literature is in the estimation of the Hubble constant H_0, between the cosmic microwave background (CMB) and the direct local distance ladder measurements. Assuming the ΛCDM scenario, Planck-CMB data analysis provides $H_0 = 67.4 \pm 0.5\ \mathrm{km\,s^{-1}\,Mpc^{-1}}$ [1], which is in 4.4σ tension with a cosmological model-independent local measurement $H_0 = 74.03 \pm 1.42\ \mathrm{km\,s^{-1}\,Mpc^{-1}}$ [2] from the *Hubble* Space Telescope (HST) observations of 70 long-period cepheids in the Large Magellanic Cloud. Additionally, a combination of time-delay cosmography from H0LiCOW lenses and the distance ladder measurements are in 5.2σ tension with the Planck-CMB constraints [3]. Recently, based on a joint analysis from several geometrical probes, a tension of $\sim 6\sigma$ was observed in [4] under the consideration of minimal theoretical assumptions. Motivated by these observational discrepancies, it has been widely discussed in the literature whether a new physics beyond the standard cosmological model can solve the H_0 tension (see [5–7] and references therein for a review). In addition to the H_0 disagreement, a significant tension between Planck data with redshift surveys data and weak lensing measurements has been reported, about the value of the matter density Ω_m and the amplitude of growth of the structures σ_8, also quantified in terms of the parameter: $S_8 = \sigma_8\sqrt{\Omega_m/0.30}$. A higher S_8 value is estimated from CMB data assuming ΛCDM, namely, $S_8 = 0.834 \pm 0.016$ [1] from Planck data and $S_8 = 0.840 \pm 0.030$ from ACT + WMAP joint analysis [8]. The cosmic shear and redshift space distortion (RSD) measurements have predicted a lower value of S_8. This tension is above the 2σ level with KiDS-450 ($S_8 = 0.745 \pm 0.039$) [9], KiDS + VIKING − 450 ($S_8 = 0.737^{+0.040}_{-0.036}$) [10], and Dark Energy Survey (DES) ($S_8 = 0.783 \pm 0.021$) [11]. The KiDS-1000 team

*jcarlos.dearaujo@inpe.br
†antonio.defelice@yukawa.kyoto-u.ac.jp
‡suresh.math@igu.ac.in
§rafadcnunes@gmail.com

reported a 3σ tension with Planck-CMB [12]. The tension becomes 3.2σ if we consider the combination of VIKING-450 and DESY1 [13] and 3.4σ for BOSS + VIKING − 450 ($S_8 = 0.728 \pm 0.026$) [14]. Also, in agreement with a lower value, there is an estimate from the BOSS Galaxy Power Spectrum $S_8 = 0.703 \pm 0.045$ [15]. See [16] and references therein for a minireview and additional information on S_8 estimations. Although this tension could be due to systematic errors, it is worthwhile to investigate the possibility of new physics beyond the standard model to explain the S_8 tension [17–29]. Additionally, the authors in [24] identified a large tension between RSD and CMB measurements. Disagreement between CMB and combinations of RSD measurements with other datasets, including the E_G statistic, is discussed in [30], pointing out a tension up to 5σ, depending on the datasets.

On the other hand, there are theoretical and observational reasons to believe that general relativity (GR) should be modified when gravitational fields are strong and/or on large scales. From an observational point of view, the physical mechanism responsible for accelerating the expansion of Universe at late times is still an open question, and it has been intensively investigated whether modified gravity scenarios can explain such an accelerated stage, as well as to fit very well with the observational data from different sources (see [31] for review). Also, theories beyond GR can serve as alternatives to explain the current H_0 tension [32–36]. One of the most interesting possibilities for modification of gravity is to give a mass to the graviton (see [37] for review about massive gravity theories). In this work, we investigate in detail the observational feasibility of the minimal theory of massive gravity (MTMG) [38,39], due to its infrared Lorentz violations measurable at cosmological scales. We robustly constrain the MTMG framework using observational probes of the $f\sigma_8$ growth rate of cosmological perturbations, which is a useful bias-free statistical cosmic test; we also combine these growth rate data with several geometric observations, such as the most recent data from type Ia supernovae and baryon acoustic oscillations. We derive and discuss observational perspectives from how the MTMG scenario predicts the statistical plane for $S_8 - \Omega_m$ in direct comparison with the ΛCDM model, as well as the potential of the model in alleviating the H_0 tension. Furthermore, we investigate for the first time how the Planck-CMB data constrain the MTMG baseline model. Our results also provide a new constraint on the graviton mass from Planck-CMB data, obtained in the MTMG context. We find that the use of Planck-CMB data selects parameter space for MTMG, which is compatible with a nonzero but positive value of $\mu^2/H_0^2 = 0.25^{+0.16}_{-0.10}$, μ being the mass of the graviton. This is probably the newest and most interesting result from this study.

This paper is structured as follows. In Sec. II, we review and introduce the MTMG scenario. In Sec. III, we present the datasets and methodology used in this work. In Sec. IV, we discuss the main results of our analysis. In Sec. V, we summarize the main findings of this study.

II. MINIMAL THEORY OF MASSIVE GRAVITY

The model we study here is a model that has been introduced in order to fix the cosmology of massive gravity, i.e., to have a stable Friedmann-Lemaître-Robertson-Walker (FLRW) background without ghosts or strong-coupling issues. The model has been introduced in order to study a standard cosmological phenomenology to the theories with a massive graviton. In order for this goal to be achieved, the theory in its simplest form (i.e., in vacuum) has only two gravitational degrees of freedom (corresponding to the two polarization gravitational waves). Furthermore, on FLRW background, MTMG shares the same background of de Rham–Gabadadze-Tolley (dRGT) [40,41]. This fact was implemented by construction in MTMG. Therefore, also MTMG is endowed, as dRGT, with two branches that are named the (1) self-accelerated branch and (2) normal branch.

These two branches have, in general, different FLRW background and perturbation dynamics. In particular, the self-accelerated branch has a phenomenology that is identical in everything to the standard ΛCDM except for the propagation of tensor modes, which are now massive (compared to GR). On the other hand, in the normal branch, we have the possibility of giving a general dynamics for the graviton mass. This allows for many phenomenological possibilities. However, in order to study this branch, it is somehow convenient to study its simplest realization, namely, the one for which the effective energy density of the MTMG component becomes a constant during the whole evolution.

More in detail, MTMG relies on the presence and choice of a three-dimensional fiducial metric, which, in unitary gauge, will be written here as $\tilde{\gamma}_{ij} = \tilde{a}^2\delta_{ij}$, where $\tilde{a} = \tilde{a}(t)$ is the fiducial scale factor. On top of that, there is need of the fiducial lapse $M = M(t)$ and of another 3D tensor $\tilde{\zeta}^i{}_j$, which represents the time variation of the fiducial vielbein (for details, see [38,39]). Out of the fiducial and physical metrics, one builds up the following quantities:

$$\mathcal{K}^k{}_n = \left(\sqrt{\tilde{\gamma}^{-1}\gamma}\right)^k_n, \tag{1}$$

$$\mathfrak{K}^k{}_n = \left(\sqrt{\gamma^{-1}\tilde{\gamma}}\right)^k_n, \tag{2}$$

$$\mathfrak{K}^k{}_n\mathcal{K}^n{}_m = \delta^k{}_m = \mathcal{K}^k{}_n\mathfrak{K}^n{}_m. \tag{3}$$

Out of these quantities, one defines the following symmetric tensor:

$$\Theta^{ij} = \frac{\sqrt{\tilde{\gamma}}}{\sqrt{\gamma}}\{c_1(\gamma^{il}\mathcal{K}^j{}_l + \gamma^{jl}\mathcal{K}^i{}_l) + c_2[\mathcal{K}(\gamma^{il}\mathcal{K}^j{}_l + \gamma^{jl}\mathcal{K}^i{}_l) - 2\tilde{\gamma}^{ij}]\} + 2c_3\gamma^{ij}, \quad (4)$$

where $c_{1,2,3}$ are constants. We then need the following building blocks:

$$\mathcal{C}_0 = \frac{1}{2}m^2 M K_{ij}\Theta^{ij} - m^2 M\left\{\frac{\sqrt{\tilde{\gamma}}}{\sqrt{\gamma}}[c_1\tilde{\zeta} + c_2(\mathcal{K}\zeta - \mathcal{K}^m{}_n\tilde{\zeta}^n{}_m)] + c_3\mathfrak{K}^m{}_n\tilde{\zeta}^n{}_m\right\}, \quad (5)$$

$$\mathcal{C}^n{}_i = -m^2 M\left\{\frac{\sqrt{\tilde{\gamma}}}{\sqrt{\gamma}}\left[\frac{1}{2}(c_1 + c_2\mathcal{K})(\mathcal{K}^n{}_i + \gamma^{nm}\mathcal{K}^l{}_m\gamma_{li}) - c_2\tilde{\gamma}^{nl}\gamma_{li}\right] + c_3\delta^n{}_i\right\}, \quad (6)$$

where γ and $\tilde{\gamma}$ represent the determinants of γ_{ij} and $\tilde{\gamma}_{ij}$, respectively. Furthermore K_{ij} is the extrinsic curvature of γ_{ij}, namely, $K_{ij} = \frac{1}{2N}(\dot{\gamma}_{ij} - \mathcal{D}_i N_j - \mathcal{D}_j N_i)$, where N is the lapse, N^i is the shift vector, and $\mathcal{D}$ is the covariant derivative compatible with the 3D metric γ_{ij}. Finally, $\mathcal{K} \equiv \mathcal{K}^n{}_n$ and $\tilde{\zeta} \equiv \tilde{\zeta}^n{}_n$. We are now ready to define the action of MTMG as follows:

$$S = S_{\rm pre} + \frac{M_{\rm P}^2}{2}\int d^4x N\sqrt{\gamma}\left(\frac{m^2}{4}\frac{M}{N}\lambda\right)^2\left(\Theta_{ij}\Theta^{ij} - \frac{1}{2}\Theta^2\right) - \frac{M_{\rm P}^2}{2}\int d^4x\sqrt{\gamma}[\lambda\mathcal{C}_0 - (\mathcal{D}_n\lambda^i)\mathcal{C}^n{}_i] + S_{\rm mat}, \quad (7)$$

where $S_{\rm mat}$ represents the standard matter action. We still need to define the last bits of the theory, which are given by

$$S_{\rm pre} = S_{\rm GR} + \frac{M_{\rm P}^2}{2}\sum_{i=1}^{4}\int d^4x\mathcal{S}_i, \quad (8)$$

$$S_{\rm GR} = \frac{M_{\rm P}^2}{2}\int d^4x N\sqrt{\gamma}[{}^{(3)}R + K^{ij}K_{ij} - K^2], \quad (9)$$

$$\mathcal{S}_1 = -m^2 c_1\sqrt{\tilde{\gamma}}(N + M\mathcal{K}), \quad (10)$$

$$\mathcal{S}_2 = -\frac{1}{2}m^2 c_2\sqrt{\tilde{\gamma}}(2N\mathcal{K} + M\mathcal{K}^2 - M\tilde{\gamma}^{ij}\gamma_{ji}), \quad (11)$$

$$\mathcal{S}_3 = -m^2 c_3\sqrt{\gamma}(M + N\mathfrak{K}), \quad (12)$$

$$\mathcal{S}_4 = -m^2 c_4\sqrt{\gamma}N. \quad (13)$$

The theory has been defined on the unitary gauge (for the Stuckelberg fields), so we cannot make any further gauge choice. In what follows, we describe the background and perturbation analysis by using the following variables. For the scalar modes, the flat 3D metric is then written according to

$$ds_3^2 = \gamma_{ij}dx^i dx^j = [a(t)^2(1+2\zeta)\delta_{ij} + 2\partial_i\partial_j E]dx^i dx^j, \quad (14)$$

a being the scale factor of the physical metric. Then we can define the lapse and shift vector as

$$N = N(t)(1+\alpha), \quad (15)$$

$$N_i = N(t)\partial_i\chi. \quad (16)$$

We also need to give

$$\lambda = \lambda(t) + \delta\lambda, \quad (17)$$

$$\lambda^i = \frac{1}{a^2}\delta^{ij}\partial_j\delta\lambda_V. \quad (18)$$

Finally, we need to give all matter actions together with their own variables.

It is possible to show that, on the background, $\lambda(t) = 0$. In this case, the dynamics of MTMG imposes the following constraint:

$$\left(HX - H\frac{M}{N} + \frac{\dot{X}}{N}\right)(X^2c_1 + 2Xc_2 + c_3) = 0, \quad (19)$$

where we have defined the variable $X \equiv \tilde{a}/a$, being the ratio between the fiducial and the physical scale factors. The function $H = \dot{a}/(aN)$ is the Hubble parameter, and the coefficients $c_{1,2,3}$ are instead constant coefficients. On solving Eq. (19), we can see that in this setup only two solutions are possible: (1) setting $X^2c_1 + 2Xc_2 + c_3 = 0$, which defines the self-accelerating branch and leads to $X = \text{const}$ and (2) the normal branch for which $M = NX + \dot{X}/H$, where the time dependence of X is still not imposed. From here onward, we will only focus on the normal branch and, in particular, we fix the dynamics of X so that $X = X_0 = \text{const}$.

As a consequence of this choice, the background equations of MTMG read as follows:

$$3M_{\rm P}^2H^2 = \sum_I\rho_I + \rho_{\rm MTMG}, \quad (20)$$

$$2M_{\rm P}^2\frac{\dot{H}}{N} = -\sum_I(\rho_I + P_I), \quad (21)$$

$$\frac{\dot{\rho}_I}{N} = -3H(\rho_I + P_I), \quad (22)$$

where $\rho_{\rm MTMG} \equiv \frac{m^2M_{\rm P}^2}{2}(c_1X_0^3 + 3c_2X_0^2 + 3c_3X_0 + c_4)$ is a constant. Here the sum over the index I is over all the

standard matter components. In this case, we can see that the background equations of motion exactly reduce to the ones of ΛCDM (endowed with an effective cosmological constant; i.e., the model is self-accelerating).

Let us now describe the dynamics of the perturbation equations of motion. We will follow here a procedure similar to the one introduced in [32,42,43]. We will have the perturbation equations of motion coming from the gravity sector (the ones for α, χ, ζ, E, $\delta\lambda$, and $\delta\lambda_V$) together with the ones coming from each matter component. We then find the equations of motion for each of the fields we have. In the following, we will (and can) set $N(t) = a(t)$ as to have dynamics in terms of the conformal time. Although we cannot fix any gauge for the perturbations, we can still perform field redefinitions. In particular, we will introduce the following ones:

$$\alpha = \psi - \frac{\dot{\chi}}{a} + \frac{1}{a}\frac{d}{dt}\left[a\frac{d}{dt}\left(\frac{E}{a^2}\right)\right], \tag{23}$$

$$\zeta = -\phi - H\chi + aH\frac{d}{dt}\left(\frac{E}{a^2}\right). \tag{24}$$

These definitions correspond to the usual gauge-invariant definitions for the Bardeen potentials ϕ and ψ. Then we will use the Newtonian gauge-invariant fields ϕ and ψ to rewrite the modified Einstein equations. For each matter component, labeled with I, we also introduce gauge-invariant combinations δ_I's and θ_I's (in place of the density contrast $\delta\rho_I/\rho_I$ and the scalar speed $u_{Ii} = \partial_i v_I$, respectively) as follows:

$$\frac{\delta\rho_I}{\rho_I} = \delta_I - \frac{\dot{\rho}_I}{a\rho_I}\chi + \frac{\dot{\rho}_I}{\rho_I}\frac{d}{dt}\left(\frac{E}{a^2}\right), \tag{25}$$

$$v_I = -\frac{a}{k^2}\theta_I + \chi - a\frac{d}{dt}\left(\frac{E}{a^2}\right). \tag{26}$$

In terms of these variables, the equations of motion for each matter component, for the lowest multipoles, read as follows:

$$\dot{\delta}_I = 3a(w_I - c_{sI}^2)H\delta_I - (1 + w_I)(\theta_I - 3\dot{\phi}), \tag{27}$$

$$\dot{\theta}_I = aH(3c_{sI}^2 - 1)\theta_I + k^2\psi + \frac{c_{sI}^2 k^2}{1 + w_I}\delta_I - k^2\sigma_I, \tag{28}$$

where $w_I \equiv P_I/\rho_I$, and $c_{sI}^2 = \left(\frac{\partial p_I}{\partial \rho_I}\right)_s$ is the speed of propagation for each matter species (i.e., $\dot{p}_I/\dot{\rho}_I$, which vanishes for dust and equals $1/3$ for photons). This result merely shows that the dynamical equations of motion for the matter components exactly coincide with the same ones in ΛCDM. This is not a surprise, as modifications of gravity only enter in the gravity sector.

The equations of motion for $\delta\lambda_V$ impose

$$\chi = -\frac{\phi}{H} + \frac{\dot{E}}{a} - 2HE. \tag{29}$$

We can solve the equations of motion for χ in terms of $\delta\lambda$ (and other fields) and the equations of motion for α in terms of E. We can consider a linear combination of the equations of motion for ζ and E in order to find a solution for $\delta\lambda_V$.

At this point, the equation of motion for $\delta\lambda$ gives

$$\mathcal{E}_0 \equiv \left[\frac{(Y\theta - 2)k^2}{a^2} + \frac{9\theta Y\Gamma}{2}\right]\phi - 3\sum_I \varrho_I\delta_I + \frac{9aH(Y\theta - 2)}{2k^2}\sum_I \Gamma_I\theta_I = 0, \tag{30}$$

where we have introduced $\rho_I = 3M_{\rm P}^2\varrho_I$, $P_I = 3M_{\rm P}^2 p_I$, $\Gamma_I \equiv \varrho_I + p_I$, $\Gamma = \sum_I \Gamma_I$, $Y = H_0^2/H^2$, and $\theta \equiv \frac{m^2 X_0}{2H_0^2}(c_1 X_0^2 + 2c_2 X_0 + c_3)$, which represents the only extra parameter that enters into the equations of motion in addition to the background effective cosmological constant. In the ΛCDM limit, whenever $|\theta Y| \ll 1$, we recover the GR standard evolution.

The equation of motion for E, the last one available in the gravity sector, gives

$$\mathcal{E}_1 \equiv \dot{\phi} + \frac{3Y\theta a\Gamma\phi}{2H(Y\theta - 2)} + aH\psi + \frac{3a^2}{k^2(Y\theta - 2)}\sum_I \Gamma_I\theta_I = 0. \tag{31}$$

On taking the time derivative of $\mathcal{E}_0$ and removing $\dot{\phi}$ from $\mathcal{E}_1$, we find the following derived equation of motion:

$$\mathcal{E}_2 \equiv \psi + \frac{9a^2}{2k^2}\sum_I \Gamma_I\sigma_I - \frac{9a^2\theta Y}{k^2(2Y\theta - 4)}\sum_I c_{sI}^2\varrho_I\delta_I - \left[1 + \frac{3\theta Y\Gamma}{(2Y\theta - 4)H^2} + \frac{27Y\theta a^2}{2k^2(2 - Y\theta)}\left(\sum_J c_{sJ}^2\Gamma_J - \frac{\Gamma^2}{2H^2}\right)\right]\phi - \frac{27\theta Y\Gamma a^3}{4k^4(Y\theta - 2)H}\sum_I \Gamma_I\theta_I = 0, \tag{32}$$

where we have also used the matter equations of motion in order to replace $\dot{\delta}_I$, etc. In the limit $|\theta Y| \to 0$, the above equations reduce to the standard GR form. We will use, as in GR, both $\mathcal{E}_1$ and $\mathcal{E}_2$ as the dynamical equations in the gravity sector. The fact that we do not have any additional dynamical equation of motion is a consequence of the fact that MTMG does not add any new dynamical degree of freedom in the theory.

Although the previous equations, never appearing before in the literature, completely define the behavior of gravity in MTMG, at any time and scale, we finish the description of the theory by considering the behavior of the theory under the influence of a single dust fluid at late times (i.e., neglecting radiation), in order to understand the effect of MTMG for the effective gravitational constant. Since this last step has already been performed in the literature (see, e.g., [39,44,45]), this last calculation can then be considered to be a check of the calculations presented so far in this paper. Then on considering a dust fluid (mimicking CDM or late-time baryons), Eqs. (27) and (28) reduce to

$$\mathcal{E}_D \equiv \dot{\delta}_c + \theta_c - 3\dot{\phi} = 0, \tag{33}$$

$$\mathcal{E}_V \equiv \dot{\theta}_c + aH\theta_c - k^2\psi = 0. \tag{34}$$

We can then solve Eq. (32) for ψ in terms of ϕ and θ_c (dust having no shear, and vanishing c_s^2). On replacing, by using Eq. (31), $\dot{\phi}$ into Eq. (33), we can then solve $\mathcal{E}_D = 0$ for θ_c in terms of ϕ and $\dot{\delta}_c$. We can now replace θ_c, ψ, and $\dot{\phi}$ (coming from $\dot{\theta}_c$) inside Eq. (34) and solve $\mathcal{E}_V = 0$ for ϕ in terms of $\dot{\delta}_c$ and $\ddot{\delta}_c$. Finally, on replacing ϕ and θ_c in Eq. (30), we find a closed second-order differential equation for δ_c. On evaluating this last equation for subhorizon scales, that is, for $k/(aH) \gg 1$, we find

$$\ddot{\delta}_c + aH\dot{\delta}_c - \frac{3}{2}\frac{G_{\rm eff}}{G_N}\varrho_c a^2 \delta_c = 0, \tag{35}$$

where $M_{\rm P}^2 = (8\pi G_N)^{-1}$, $\Omega_c = \varrho_c(t)/H^2$, and

$$\frac{G_{\rm eff}}{G_N} = \frac{2}{2-\theta Y} - \frac{3\theta Y \Omega_c}{(2-\theta Y)^2}, \tag{36}$$

matching the result found, e.g., in [44]. The same dynamical equation holds also for the late-time baryonic fluid. Since we are going to use bounds on integrated Sachs-Wolfe (ISW) galaxy cross-correlations, it is worthy to find the expression for the ISW field, defined as $\psi_{\rm ISW} \equiv \phi + \psi$, in the subhorizon scales approximation. We find that

$$\psi_{\rm ISW} = -\frac{3H_0^2\Omega_{m0}}{k^2}\frac{\Sigma\delta_m}{a}, \tag{37}$$

$$\Sigma \equiv \frac{8-(4+3\Omega_m)\theta Y}{2(2-\theta Y)^2}, \tag{38}$$

where here $\Omega_m = \Omega_m(t) = \rho_m/(3M_{\rm P}^2H^2)$, and $\Omega_{m0} = \Omega_m(z=0)$ (in the next sections, unless specified otherwise, Ω_m will be used to rewrite Ω_{m0}). This result for $\psi_{\rm ISW}$ agrees with the one found in [45].

Let us finally discuss the equations of motion for the gravitational waves propagating on this flat FLRW background (the vector modes do not show any deviation from GR). In fact, the contribution of MTMG to the tensor modes consists, by construction (see, e.g., [38,39]), of introducing a nonzero squared mass $\mu^2 = H_0^2\theta$ to them. The equations of motion for the two tensor modes polarizations (h_f labeled with $f \in \{+,\times\}$) become

$$\ddot{h}_f = -2\frac{\dot{a}}{a}\dot{h}_f - (k^2 + \theta H_0^2 a^2)h_f, \tag{39}$$

where on the right-hand side a source term can further be added.

We implemented the model described above in the CLASS code [46]. In Fig. 1, we quantify the MTMG model affects on the CMB temperature power spectrum, i.e., C_l^{TT}, with respect to GR-ΛCDM prediction. We can see that increasing θ enhances the CMB temperature power spectrum at low l. This effect is well known for dark energy and massive gravity (MG) models, and it is due to the integrated Sachs-Wolfe effect, which affects the CMB spectrum at low l, but has no significant effect at large scales. For scales larger than $l > 100$, we note $C_l^{GR,TT} \approx C_l^{\rm MTMG,TT}$. In Fig. 2, we show the difference on the $P(k,z)$ at four different redshift values on the scales $k \in [10^{-4}, 1]$ h/Mpc. These z values are chosen because our RSD sample covers the range $z \in [0.02, 1.94]$. For a quantitative example, taking

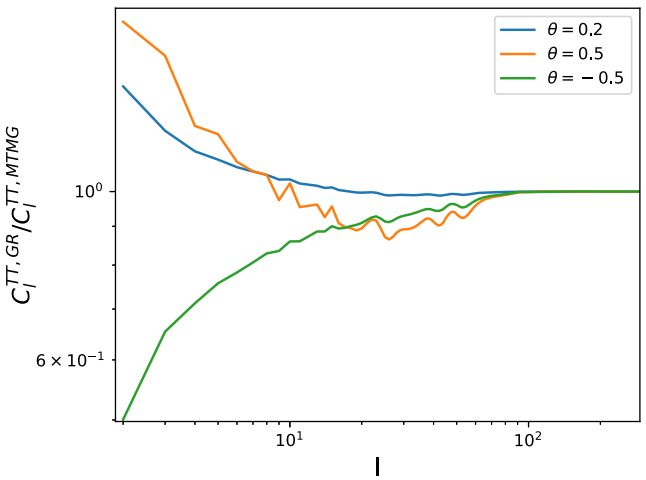

FIG. 1. Deviations of the CMB TT power spectrum for ΛCDM from MTMG for some values of θ.

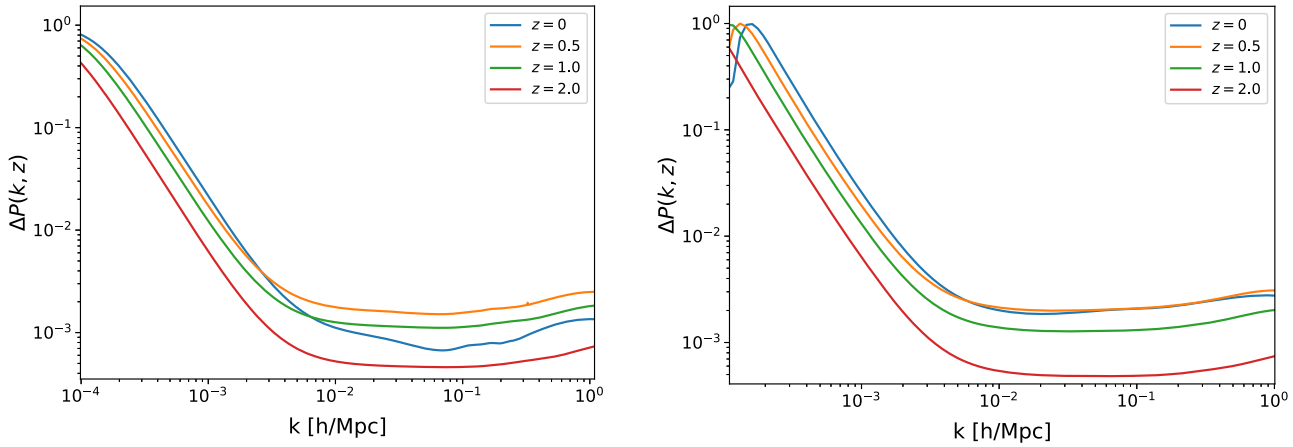

FIG. 2. Left: deviations of the matter power spectrum, $\Delta P(k,z) = |P(k,z)^{\rm MTMG} - P(k,z)^{GR}|/(P(k,z)^{\rm MTMG} + P(k,z)^{GR})$, for ΛCDM from MTMG with $\theta = -0.2$ for some values of z. Right: same as on the left, but assuming $\theta = 0.2$.

$\theta = -0.2$, we find that the difference with respect to ΛCDM is ∼25% at $k = 10^{-3}$ h/Mpc, while for $k > 10^{-2}$ h/Mpc the difference is <0.2%, for all z values. For the case with $\theta = 0.2$, we note that for $k > 10^{-3}$ h/Mpc, we have a similar difference as in the previous case, but with different $P(k,z)$ behavior at different z values, as expected, since the dynamics depends on the signal in θ. For scales $k < 10^{-3}$, significant deviations are noted. It is important to mention that on very large scales, the cosmic variance effects can be significant. In these simulations, the predictions of the nonlinear effects are performed using the HMcode code [47]. Nonlinear dynamics of the MTMG framework using N-body simulations were investigated in detail in [48].

III. DATA AND METHODOLOGY

In this section, we present the datasets and methodology used to obtain the observational constraints on the model parameters by performing Bayesian Markov chain Monte Carlo analysis. In order to constrain the parameters, we use the following datasets.

CMB.—We use the full Planck-2018 [1] CMB temperature and polarization data which comprise the low-l temperature and polarization likelihoods at $l \leq 29$, temperature (TT) at $l \geq 30$, polarization power spectra, and cross-correlation of temperature and polarization, while also including the Planck-2018 CMB lensing power spectrum likelihood [49] in our analysis.

RSD.—The growth rate data comprise $f(z)\sigma_8(z)$ measurements from a variety of redshift space distortion surveys. The current measurements of $f\sigma_8(z)$ come from a plethora of different surveys with different assumptions and systematics, thus an approach to study the statistical properties and robustness of the data is imperative. In [50], an internal robustness analysis was used to validate a subset of $f\sigma_8(z)$ measurements. In our analysis, we use the compilation of the $f\sigma_8(z)$ measurements presented in Table I in [50], which are minimally affected by systematic-contaminated data points. We refer to this dataset as the dataset of RSD measurements. To build the likelihood function, we follow the same methodology as presented in [51]. It is important to highlight that the RSD sample is still fiducial to some cosmology, for example, fixed on a ΛCDM baseline, different assumptions on the reference value of Ω_m, and nonlinearities modeling of which starts to play an important role on smaller scales and at later epochs. These points should be taken into account to accurately estimate the cosmological parameters. Our sample is minimally affected by systematic-contaminated $f\sigma 8$ data points, checked through the Bayesian model comparison framework described in [50], identifying potential outliers as well as subsets of data affected by systematics or new physics.

BAO.—The baryon acoustic oscillations (BAOs) provide an important cosmological probe, which can trace expanding spherical waves of baryonic perturbations from acoustic oscillations at recombination time through the large-scale

TABLE I. Constraints at 95% C.L. on Ω_m, σ_8, S_8, and $\theta = \mu^2/H_0^2$, inferred from different dataset combinations, in the MTMG model.

Dataset	θ	Ω_m	σ_8	S_8
RSD	$-5.2^{+7.1}_{-4.8}$	$0.37^{+0.17}_{-0.16}$	$0.808^{+0.086}_{-0.084}$	$0.89^{+0.19}_{-0.20}$
RSD + BAO + Pantheon	$-1.8^{+3.3}_{-4.4}$	$0.305^{+0.041}_{-0.039}$	$0.796^{+0.091}_{-0.073}$	$0.802^{+0.10}_{-0.096}$
RSD + BAO + Pantheon + ISW	$-0.12^{+0.28}_{-0.26}$	$0.293^{+0.018}_{-0.018}$	$0.775^{+0.055}_{-0.055}$	$0.766^{+0.057}_{-0.055}$

structure correlation function. In this work, we consider the most recent BAO data compilation composed of the $D_V(z)/r_d$, $D_M(z)/r_d$, and $D_H(z)/r_d$ measurements compiled in Table III in [52], regarding BAO-only data.

Pantheon.—The supernovae type Ia have traditionally been one of the most important astrophysical tools in establishing the so-called standard cosmological model. For the present analysis, we use the Pantheon compilation, which consists of 1048 SN Ia distributed in the redshift range $z \in [0.01, 2.3]$ [53].

ISW.—The late-time integrated Sachs-Wolfe effect on the CMB is an effect imprinted in the angular pattern of the CMB in the presence of a time-varying cosmological gravitational potential, which can be due to a nonflat universe [54], as well as for a flat one in the presence of dark energy or modified gravity theories [55–57]. A nonzero ISW necessarily implies the presence of a generating physical source for the accelerated expansion of the Universe at late times. For the present analysis, we use the cross-correlation of the CMB with galaxy surveys that derive constraints on the ISW as obtained in [58]. We use the five catalogs of extragalactic sources as presented in [58], namely, the 2MASS Photometric Redshift catalog, the WISE SuperCOSMOS photo-z catalog, the NRAO VLA Sky Survey radio sources catalog, and the SDSS DR12 and SDSS DR6 QSO photometric catalogs.

We use the Metropolis-Hastings mode in CLASS+ MONTEPYTHON code [46,59,60] to derive the constraints on cosmological parameters using various data combinations from the datasets described above, ensuring a Gelman-Rubin convergence criterion of $R - 1 < 10^{-3}$. In what follows, we describe our main results.

IV. RESULTS AND DISCUSSIONS

We divide the analysis into two parts. First, we consider RSD and RSD + BAO + Pantheon data, that is, the growth data and its combination with the geometric data. Thus, we can quantify the dynamics of the model and the constraints on θ without CMB data influence. It is important to check the prediction of the model about σ_8 or S_8 in the absence of the CMB data. Then, we add ISW information to these data. In the second round of analysis, we analyze the model with CMB data and discuss the potential of the model to solving and/or alleviating the H_0 and S_8 tensions.

A. Analysis with the growth, geometric, and ISW data

Modelwise, we consider $\Lambda\text{CDM} + \theta$ model baseline, spanned by the five parameters: the Hubble constant H_0 or, equivalently, the reduced Hubble constant $h \equiv H_0/(100\ \mathrm{km\,s^{-1}\,Mpc^{-1}})$, the physical baryon density $\omega_b \equiv \Omega_b h^2$, the physical cold dark matter density $\omega_c \equiv \Omega_c h^2$, σ_8, and θ, quantifying deviations from GR. The matter density parameter today Ω_m is derived by $\Omega_m = \Omega_b + \Omega_c$. Another important derived parameter is $S_8 \equiv \sigma_8\sqrt{\Omega_m/0.3}$. To constrain the physical baryon density, we adopt a Gaussian prior on ω_b from big bang nucleosynthesis: $100\omega_b = 2.233 \pm 0.036$ [61]. So that the tensor modes do not develop instability with a timescale shorter than the age of the Universe, we impose the prior $\theta \geq -10$. In the limit $\theta = 0$, we recover the evolution equation for the perturbations as in GR. Note that the ΛCDM and MTMG models are indistinguishable at the background evolution. Thus, the data combination BAO + Pantheon is indistinguishable for both scenarios. We use BAO + Pantheon to break the statistical degeneracy on Ω_m, which may be present when considering RSD data only. Since both ΛCDM and MTMG models can predict different constraints on Ω_m in light of only the RSD data, breaking this background degeneracy with BAO + Pantheon can significantly improve the results. Finally, we also consider ISW sample data. Table I summarizes the main results of our statistical analyses.

Figure 3, on the left panel, shows the parameter space in the $S_8 - \Omega_m$ plane at 68% and 95% C.L. with various datasets in ΛCDM and MTMG models. First, we note that, in direct comparison with the constraints provided with ΛCDM, the MTMG model can provide an enlargement in both S_8 and Ω_m estimations. The right panel shows the regions at 68% and 95% C.L. in the $\theta - \Omega_m$ plane with RSD and RSD + BAO + Pantheon data in the MTMG model. We find $\theta = -5.2^{+7.1}_{-4.8}$, $\theta = -1.8^{+3.3}_{-4.4}$ and $\theta = -0.12^{+0.28}_{-0.26}$ at 95% C.L. from RSD, RSD + BAO+ Pantheon, and RSD + BAO + Pantheon + ISW data, respectively. The addition of the ISW data improves the constraints on θ because θ can significantly affect the late-time ISW effect [45]. So, ISW data improve θ and, consequently, by correlation, improvements on the other parameters in the baseline are also reached, which are already well constrained from other datasets. The joint analysis with RSD + BAO + Pantheon + ISW data provides robust and accurate constraints on the theory using only late-time probes. As we will show in the next section, the constraints are further improved with the addition of

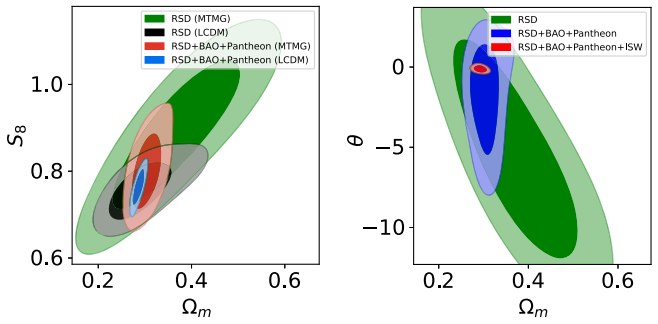

FIG. 3. Left: 68% and 95% confidence levels on the $S_8 - \Omega_m$ plane from various datasets in ΛCDM and MTMG models. Right: 68% and 95% confidence levels on the $\theta - \Omega_m$ plane from various datasets in MTMG model. GR is recovered for $\theta = 0$.

CMB data. All these constraints are consistent with the GR prediction, i.e., $\theta = 0$ even at 68% C.L. For comparison, assuming ΛCDM cosmology, from RSD data, we find $\Omega_m = 0.293^{+0.10}_{-0.083}$ and $S_8 = 0.758^{+0.082}_{-0.073}$. From the joint analysis with RSD + BAO + Pantheon data, we find $\Omega_m = 0.286^{+0.015}_{-0.015}$ and $S_8 = 0.765^{+0.055}_{-0.054}$. We can clearly see that the addition of BAO + Pantheon improves the constraint by breaking down the degeneracy on Ω_m, in both models, i.e., ΛCDM and MTMG. As we will see in the next section, in the MTMG model, there is no tension in the $S_8 - \Omega_m$ plane, when analyzed from CMB and RSD data. Therefore, MTMG brings an agreement between these data.

B. MTMG in the light of CMB data

For the first time, here we find the constraints on the MTMG model from the full Planck-CMB dataset alone and its combination with several other data. The baseline seven free parameters set of the MTMG model is given by

$$\mathcal{P} = \{\omega_{\rm b}, \omega_{\rm cdm}, \theta_s, \ln(10^{10}A_s), n_s, \tau_{\rm reio}, \theta\},$$

where the first six parameters are the baseline parameters of the standard ΛCDM model, namely, $\omega_{\rm b}$ and $\omega_{\rm cdm}$ are, respectively, the dimensionless densities of baryons and cold dark matter, θ_s is the ratio of the sound horizon to the angular diameter distance at decoupling, A_s and n_s are, respectively, the amplitude and spectral index of the primordial curvature perturbations, and $\tau_{\rm reio}$ is the optical depth to reionization. As commented before, the parameter θ quantifies deviations from GR induced by the MTMG framework.

Table II displays summary of our statistical analyses using the full Planck-CMB dataset and its combination with several other datasets. In the last column, the full joint analysis stands for CMB + BAO + Pantheon+ RSD + ISW. Figure 4, on the left panel (right panel), shows the parameter space in the $S_8 - H_0$ ($\theta - \Omega_m$) plane,

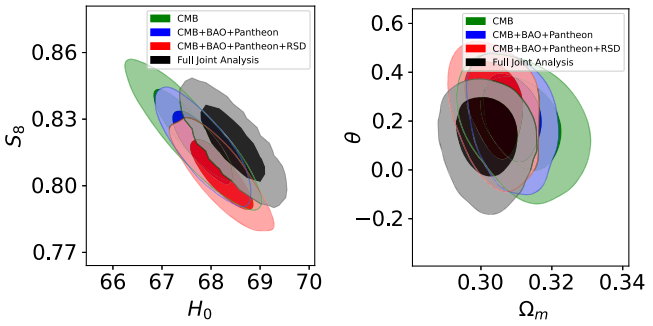

FIG. 4. Left: 68% and 95% C.L. in the $S_8 - H_0$ plane from various datasets in the MTMG model. Right: same as on the left, but in the $\theta - \Omega_m$ plane. GR is recovered for $\theta = 0$.

at 68% and 95% C.L. from the Planck-CMB dataset and its combination with other data.

In all the analyses carried out here, we note that θ can be non-null at 68% C.L., but consistent with $\theta = 0$ at 95% C.L. Thus, we do not find any significant evidence for deviations from GR. In the full joint analysis, we obtain $\theta = 0.25^{+0.16}_{-0.10}$ at 68% C.L. The constraints on MTMG using the CMB data alone are well consistent with the ΛCDM baseline. Despite θ being non-null at 68% C.L., all other parameters do not show significant deviation from the ΛCDM baseline. When BAO + Pantheon and BAO + Pantheon + RSD are added, we notice a minor shift of Ω_m to low values and H_0 to high values. This behavior is clear in Fig. 4. On the other hand, these data are known to be in tension ($\sim 3\sigma$) within ΛCDM [30]. Thus, we can combine CMB and RSD in the MTMG scenario. In other words, there is no tension in the $S_8 - \Omega_m$ plane for the MTMG model.

We know that MTMG affects the CMB spectrum predominantly at low l, and practically no effects are observed at high l. Thus, we also consider ISW data in combination with the datasets described above. We find

TABLE II. Summary of the 1σ constraints on the baseline parameters of the MTMG scenario from CMB and its combination with several other datasets. In the last column, the full joint analysis means CMB + BAO + Pantheon + RSD + ISW. The parameter H_0 is measured in the units of km s^{-1} Mpc^{-1}.

Parameter	CMB	CMB + BAO + Pantheon	CMB + BAO + Pantheon + RSD	Full joint analysis
$10^2\omega_b$	2.242 ± 0.015	2.245 ± 0.013	2.252 ± 0.013	2.247 ± 0.013
$\omega_{\rm cdm}$	0.1195 ± 0.0012	0.11903 ± 0.00090	0.11819 ± 0.00090	0.11886 ± 0.00095
$100\theta_{\rm s}$	1.04195 ± 0.00029	1.04197 ± 0.00028	1.04202 ± 0.00028	1.04197 ± 0.00028
$\ln 10^{10}A_{\rm s}$	3.042 ± 0.014	3.042 ± 0.014	3.035 ± 0.014	3.036 ± 0.015
$n_{\rm s}$	0.9663 ± 0.0044	0.9672 ± 0.0036	0.9692 ± 0.0039	0.9681 ± 0.0037
$\tau_{\rm reio}$	0.0538 ± 0.0071	0.0542 ± 0.0071	0.0520 ± 0.0070	0.0517 ± 0.0075
θ	$0.19^{+0.14}_{-0.10}$	$0.21^{+0.13}_{-0.10}$	$0.26^{+0.14}_{-0.10}$	$0.129^{+0.13}_{-0.088}$
$\Omega_{\rm m}$	0.3115 ± 0.0077	0.3089 ± 0.0054	0.3038 ± 0.0054	0.3018 ± 0.0056
H_0	67.65 ± 0.57	67.84 ± 0.40	68.22 ± 0.42	68.44 ± 0.43
σ_8	0.8071 ± 0.0064	0.8057 ± 0.0065	0.8001 ± 0.0060	0.8169 ± 0.0068
S_8	0.822 ± 0.014	0.818 ± 0.011	0.805 ± 0.010	0.819 ± 0.011

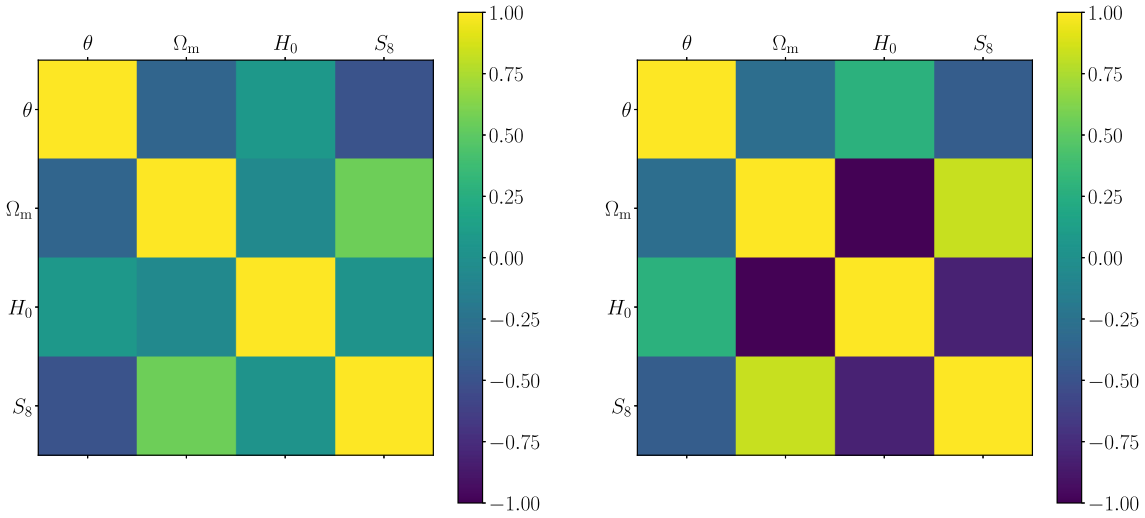

FIG. 5. Left: scatter plot quantifying the correlations for some parameters of interest in MTMG model from the RSD + BAO + Pantheon + ISW data. Right: same as the left, but for CMB + RSD + BAO + Pantheon + ISW data.

$H_0 = 68.44 \pm 0.43$ km s^{-1} Mpc^{-1} from CMB + BAO + Pantheon + RSD + ISW data. This constraint minimizes the H_0 tension up to 3.5σ compared to cosmological model-independent local measurement of H_0 from the HST observations [2]. From our joint analysis, we have $\Omega_{\rm m} = 0.301 \pm 0.0056$ and $\sigma_8 = 0.8169 \pm 0.0068$, which represents a deviation to low (high) values on $\Omega_{\rm m}$ (σ_8), respectively, compared to the CMB only constraints.

Figure 5 shows a scatter plot for the correlations between the parameters of interest in our model from the RSD + BAO + Pantheon + ISW and CMB + RSD + BAO + Pantheon + ISW data. We note that, in both cases, θ exhibits negative, positive, and negative correlations with Ω_m, H_0, and S_8, respectively. We found similar correlations in other analyses as well. Despite all the constraints on θ, from the different analyses performed here be statistically consistent with each other, it is interesting to note that θ shows a best-fit preference to $\theta < 0$ from RSD + BAO + Pantheon + ISW, and $\theta > 0$ when we add the CMB data. We know that $\theta < 0$ causes a suppression on the amplitude of the matter perturbations. This suppression behavior is necessary to fit well, for instance, with the RSD data and its combination with the BAO + Pantheon sample. On the other hand, in light of these data, the parameter θ is degenerate with the other baseline parameters. Thus, it is expected that, in the presence of RSD data with BAO + Pantheon + ISW data, preference exists for $\theta < 0$ values while not excluding the possibility of $\theta > 0$ values. Next, the addition of CMB data is expected to yield a tight constraint on θ. We find in this case that the correlation of θ with Ω_m, H_0, and S_8, increases. It is quantified in Fig. 5 comparing both panels. That increase especially occurs on Ω_m and H_0, where the correlation with H_0 increases 400%. Note that H_0 is strongly constrained using CMB data; in the MTMG model, H_0 is constrained to 0.6% accuracy. The global constraint on θ is also very tight, and the best fit on θ changes the signal due to the correlation change in the analysis RSD + BAO + Pantheon + ISW to CMB+ RSD + BAO + Pantheon + ISW. That is caused by the addition of the CMB data. We also note from the joint analysis CMB + RSD + BAO + Pantheon + ISW that $\theta > 0$ at 68% C.L. Changes in the other baseline parameters are understandable looking at Fig. 5.

It is interesting to note that CMB data can break the degeneracy present in RSD and BAO + Pantheon + RSD data, providing a tight constraint on θ when all these data are combined. It is clear from a comparison between the Tables I and II. Using the relation $\mu^2 = H_0^2\theta$, and constraints on H_0, we can infer direct constraints on the graviton mass. Figure 6, in the right panel, shows the constraint on the graviton mass squared from CMB alone, CMB+ BAO+Pantheon, CMB+BAO+Pantheon+RSD, and CMB + BAO + Pantheon + RSD + ISW. If we take an inference with prior $\mu^2 \geq 0$, we find the bound

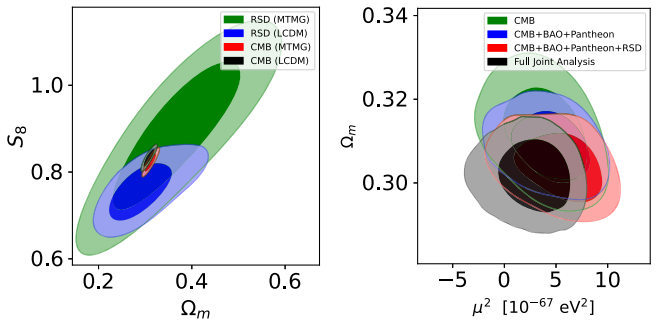

FIG. 6. Left: 68% and 95% C.L. on the parametric space $S_8 - \Omega_m$ from CMB and RSD datasets under the ΛCDM and MTMG model assumptions. Right: 68% and 95% C.L. on the parametric space $\mu^2 - \Omega_m$ from several different datasets.

$\mu \lessapprox 4 \times 10^{-34}$, $\lessapprox 4.4 \times 10^{-34}$, $\lessapprox 4.8 \times 10^{-34}$, and $\lessapprox 3.4 \times 10^{-34}$ eV at 95% C.L. from CMB alone, CMB + BAO+ Pantheon, CMB + BAO + Pantheon + RSD, and CMB+ BAO + Pantheon + RSD + ISW, respectively. Without loss of generality, this inference on μ can be performed for the other datasets. We chose to perform only using the most accurate measurements.

Our constraints are consistent with the bound $\mu < 10^{-23}$ eV on the graviton mass set by the LIGO Collaboration [62]. Bounds from the Solar System tests provide $\mu < 10^{-24}$ eV [63]. Analyzing Galactic dynamics under n-body simulations, it was shown that $\mu < 10^{-26}$ eV [64]. Constraints from observation-derived energy condition bounds show that $\mu < 10^{-31}$ eV [65]. Recently, using 14 well-timed binary pulsars, from their intrinsic orbital decay rates, the authors in [66] found $\mu < 10^{-28}$ eV. Primordial gravitational waves modeled with a massive graviton will induce extra effects on the B-mode polarization of the CMB at low-l scales, which can place a bound on the massive graviton to $\mu < 10^{-30}$ eV [67]. A more strong bound can be imposed from weak gravitational lensing observations [68] and lunar laser ranging experiments [69], viz., $\mu < 10^{-32}$ eV. In Table I in [70], the authors provide a compilation of several bounds on the graviton mass. Although found for a given (but realistic and stable) model describing a massive graviton, our constraint on the graviton mass is complementary and some orders of magnitude stronger than the previous ones. We refer to [44] for other bounds on μ in MTMG.

V. FINAL REMARKS

Despite the ΛCDM successes, some challenges at both the theoretical and observational levels have placed the ΛCDM cosmology in crossroads. At the observational level, it faces, in particular, the H_0 and growth tensions. The growth tension is based on the fact that the observed growth of cosmological perturbations at low z is weaker than the growth predicted by the standard Planck-ΛCDM parameter values. In this work, we have investigated in detail the MTMG model in the light of different observational datasets. In particular, we have derived constraints on the MTMG using Planck-CMB data for the first time. From our full joint analysis, we have found $\mu^2/H_0^2 = 0.25^{+0.16}_{-0.10}$, with μ being the mass of the graviton. It represents a non-null measurement on μ at 68% C.L.

From the theoretical side, in obtaining our results, we have considered the scalar and tensor perturbative effects under a FLRW metric, while the background evolution is equivalent to the ΛCDM model as described in Sec. II. We know that the H_0 value from CMB data depends on the angular scale $\theta_* = d_s^*/D_A^*$, where d_s^* is the sound horizon at decoupling (the distance traveled by a sound wave from the big bang to the epoch of the CMB-baryons decoupling) and D_A^* is the angular diameter distance at decoupling, which in turn depends on the expansion history $H(z)$ after decoupling, controlled also by the ratio Ω_m/Ω_{de} and H_0 mainly. In its simplest form, the MTMG scenario does not lead to changes in $H(z)$ evolution with regard to the ΛCDM model. Thus, significant changes on H_0 that are obtained in other models in the literature are not observed here. All changes on H_0 as well as on the full baseline are due to the changes on the evolution of the scalar potentials ϕ and ψ in Einstein's field equations. Within this framework, we have found that the current H_0 tension at 4.4σ can be reduced to 3.5σ. It does not completely solve this tension, but leads us to conclude that the possibility for a non-null μ can affect the cosmological parameters estimation to the CMB level too. Going beyond the simplest implementation of the MTMG model, namely, changing also $H(z)$, may address this point more significantly. It may be interesting, in a future communication, to verify massive theories with change on the background evolution, which certainly should reduce the H_0 tension significantly. We also conclude that the well-known tension on the S_8 parameter can be solved in the MTMG model, as shown in the previous section. Recently, the weak lensing and galaxy clustering measurements from the Dark Energy Survey have been updated, providing new and robust estimates on S_8, viz., $S_8 = 0.776^{+0.017}_{-0.017}$ and $S_8 = 0.812^{+0.012}_{-0.012}$ (DES + CMB) [71,72], within a ΛCDM baseline. It is interesting to interpret that the MTMG scenario, without using the CMB data, predicts $S_8 = 0.802 \pm 0.06$, while enlarging the error bar a bit, in general, on the $S_8 - \Omega_m$ plane compared to ΛCDM. Thus, comparing with DES constraint within ΛCDM baseline results, we can postulate that MTMG can also solve the S_8 tension between DES and CMB, which is around 2.3σ.

We simulate an addition of the DES and Kilo-Degree Survey (KiDS-1000) data on our full joint analysis by adding Gaussian priors on S_8 to our analysis. Figure 7, in the left panel, shows the parameter space in the $S_8 - \mu^2$ plane under the prior $S_8 = 0.776 \pm 0.017$ from the DES results [71]. In the right panel, we show the results assuming the prior $S_8 = 0.759^{+0.024}_{-0.021}$ from the KiDS-1000 data [73]. In both cases, we note that the amplitude in S_8 decreases and slightly extends the expectation of the graviton mass, but is consistent with all other results developed here. Of course, an analysis within the MTMG baseline using the full DES and KiDS likelihoods must confirm this prediction. We hope to provide such investigation in a future communication.

Therefore, in this work, we conclude that the MTMG is very well consistent with the CMB observations, as well as with other observational ones that are sensitive to the cosmological perturbation theory. Undoubtedly, the MTMG model is a viable candidate among the modified gravity theories.

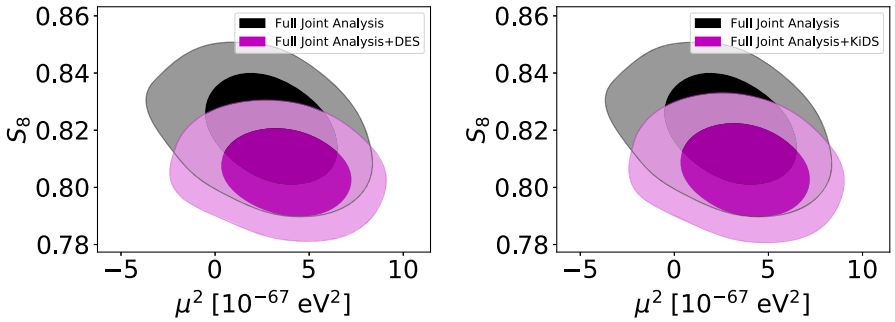

FIG. 7. Left: 68% and 95% C.L. on the parametric space $S_8 - \mu^2$ from our full joint analysis combined with a Gaussian prior on S_8 from DES results [71]. Right: Same as on the left, but the S_8 prior from KiDS-1000 [73].

ACKNOWLEDGMENTS

J. C. N. A. thanks FAPESP (2013/26258-4) and CNPq (308367/2019-7) for partial financial support. The work of A. D. F. was supported by Japan Society for the Promotion of Science Grants-in-Aid for Scientific Research Grant No. 20K03969. S. K. gratefully acknowledges the support from SERB-DST Project No. EMR/2016/000258. R. C. N. would like to thank the agency FAPESP for financial support under Project No. 2018/18036-5. Part of the numerical computation in this work was carried out at the Yukawa Institute Computer Facility.

[1] N. Aghanim, Y. Akrami, M. Ashdown, J. Aumont, C. Baccigalupi, M. Ballardini, A. J. Banday, R. B. Barreiro, N. Bartolo *et al.*, Planck 2018 results, Astron. Astrophys. **641**, A6 (2020).

[2] A. G. Riess, S. Casertano, W. Yuan, L. M. Macri, and D. Scolnic, Large magellanic cloud cepheid standards provide a 1% foundation for the determination of the hubble constant and stronger evidence for physics beyond ΛCDM, Astrophys. J. **876**, 85 (2019).

[3] K. C. Wong, S. H. Suyu, G. C.-F. Chen, C. E. Rusu *et al.*, H0licow–XIII. A 2.4 per cent measurement of H_0 from lensed quasars: 5.3σ tension between early- and late-Universe probes, Mon. Not. R. Astron. Soc. **498**, 1420 (2020).

[4] A. Bonilla, S. Kumar, and R. C. Nunes, Measurements of H_0 and reconstruction of the dark energy properties from a model-independent joint analysis, Eur. Phys. J. C **81**, 127 (2021).

[5] E. Di Valentino and L. A. e. a. Anchordoqui, Snowmass2021: Letter of interest cosmology intertwined II: The hubble constant tension, Astropart. Phys. **131**, 102605 (2021).

[6] E. D. Valentino, O. Mena, S. Pan, L. Visinelli, W. Yang, A. Melchiorri, D. F. Mota, A. G. Riess, and J. Silk, In the realm of the Hubble tension—a review of solutions, Classical Quant. Grav. **38**, 153001 (2021).

[7] L. Perivolaropoulos and F. Skara, Challenges for ΛCDM: An update, arXiv:2105.05208.

[8] S. Aiola, E. Calabrese, L. Maurin, S. Naess, B. L. Schmitt, M. H. Abitbol, G. E. Addison, P. A. R. Ade, D. Alonso, M. Amiri *et al.*, The Atacama Cosmology Telescope: DR4 maps and cosmological parameters, J. Cosmol. Astropart. Phys. 12 (2020) 047.

[9] S. Joudaki, A. Mead, C. Blake, A. Choi, J. de Jong, T. Erben, I. Fenech Conti, R. Herbonnet, C. Heymans, H. Hildebrandt *et al.*, Kids-450: Testing extensions to the standard cosmological model, Mon. Not. R. Astron. Soc. **471**, 1259 (2017).

[10] S. Joudaki, C. Blake, A. Johnson *et al.*, Kids-450 + 2dflens: Cosmological parameter constraints from weak gravitational lensing tomography and overlapping redshift-space galaxy clustering, Mon. Not. R. Astron. Soc. **474**, 4894 (2018).

[11] M. Troxel, N. MacCrann, J. Zuntz *et al.*, Dark energy survey year 1 results: Cosmological constraints from cosmic shear, Phys. Rev. D **98**, 043528 (2018).

[12] C. Heymans, T. Trster, M. Asgari *et al.*, Kids-1000 cosmology: Multi-probe weak gravitational lensing and spectroscopic galaxy clustering constraints, Astron. Astrophys. **646**, A140 (2021).

[13] M. Asgari, T. Trster, C. Heymans *et al.*, Kids+viking-450 and Des-Y1 combined: Mitigating baryon feedback uncertainty with Cosebis, Astron. Astrophys. **634**, A127 (2020).

[14] T. Trster, A. G. Snchez *et al.*, Cosmology from large-scale structure, Astron. Astrophys. **633**, L10 (2020).

[15] M. M. Ivanov, M. Simonovi, and M. Zaldarriaga, Cosmological parameters from the boss galaxy power spectrum, J. Cosmol. Astropart. Phys. 05 (2020) 042.

[16] E. Di Valentino, L. A. Anchordoqui *et al.*, Cosmology intertwined III: $f\sigma_8$ and S_8, Astropart. Phys. **131**, 102604 (2021).

[17] S. Kumar, R. C. Nunes, and S. K. Yadav, Dark sector interaction: A remedy of the tensions between CMB and LSS data, Eur. Phys. J. C **79**, 576 (2019).
[18] S. Kumar, R. C. Nunes, and S. K. Yadav, Testing the warmness of dark matter, Mon. Not. R. Astron. Soc. **490**, 1406 (2019).
[19] G. Lambiase, S. Mohanty, A. Narang, and P. Parashari, Testing dark energy models in the light of σ_8 tension, Eur. Phys. J. C **79**, 141 (2019).
[20] B. J. Barros, T. Barreiro, T. Koivisto, and N. J. Nunes, Testing $f(q)$ gravity with redshift space distortions, Phys. Dark Universe **30**, 100616 (2020).
[21] G. F. Abellan, R. Murgia, V. Poulin, and J. Lavalle, Hints for decaying dark matter from S_8 measurements, arXiv:2008.09615.
[22] S. Heimersheim, N. Schneberg, D. C. Hooper, and J. Lesgourgues, Cannibalism hinders growth: Cannibal dark matter and the S_8 tension, J. Cosmol. Astropart. Phys. 12 (2020) 016.
[23] G. j. Choi, T. T. Yanagida, and N. Yokozaki, A model of interacting dark matter and dark radiation for H_0 and σ_8 tensions, J. High Energy Phys. 01 (2021) 127.
[24] F. Skara and L. Perivolaropoulos, Tension of the E_G statistic and redshift space distortion data with the Planck-ΛCDM model and implications for weakening gravity, Phys. Rev. D **101**, 063521 (2020).
[25] V. Marra and L. Perivolaropoulos, A rapid transition of $g_{\rm eff}$ at $z_t \simeq 0.01$ as a solution of the hubble and growth tensions, Phys. Rev. D **104**, L021303 (2021).
[26] S. Kumar, Remedy of some cosmological tensions via effective phantom-like behavior of interacting vacuum energy, Phys. Dark Universe **33**, 100862 (2021).
[27] M. Lucca, Dark energy-dark matter interactions as a solution to the S_8 tension, arXiv:2105.09249.
[28] W. Yang, E. Di Valentino, S. Pan, and O. Mena, Emergent dark energy, neutrinos and cosmological tensions, Phys. Dark Universe **31**, 100762 (2021).
[29] W. Yang, E. Di Valentino, O. Mena, and S. Pan, Dynamical dark sectors and neutrino masses and abundances, Phys. Rev. D **102**, 023535 (2020).
[30] R. C. Nunes and S. Vagnozzi, Arbitrating the S_8 discrepancy with growth rate measurements from redshift-space distortions, Mon. Not. R. Astron. Soc. **505**, 5427 (2021).
[31] M. Ishak, Testing general relativity in cosmology, Living Rev. Relativity **22**, 1 (2019).
[32] A. De Felice, S. Mukohyama, and M. C. Pookkillath, Addressing H_0 tension by means of VCDM, Phys. Lett. B **816**, 136201 (2021).
[33] M. Ballardini, M. Braglia, F. Finelli, D. Paoletti, A. A. Starobinsky, and C. Umilt, Scalar-tensor theories of gravity, neutrino physics, and the H_0 tension, J. Cosmol. Astropart. Phys. 10 (2020) 044.
[34] R. C. Nunes, Structure formation in $f(t)$ gravity and a solution for H_0 tension, J. Cosmol. Astropart. Phys. 05 (2018) 052.
[35] R. DAgostino and R. C. Nunes, Measurements of H_0 in modified gravity theories: The role of lensed quasars in the late-time Universe, Phys. Rev. D **101**, 103505 (2020).
[36] A. D. Felice, C.-Q. Geng, M. C. Pookkillath, and L. Yin, Reducing the H_0 tension with generalized Proca theory, J. Cosmol. Astropart. Phys. 08 (2020) 038.
[37] C. de Rham, Massive gravity, Living Rev. Relativity **17**, 7 (2014).
[38] A. De Felice and S. Mukohyama, Minimal theory of massive gravity, Phys. Lett. B **752**, 302 (2016).
[39] A. D. Felice and S. Mukohyama, Phenomenology in minimal theory of massive gravity, J. Cosmol. Astropart. Phys. 04 (2016) 028.
[40] C. de Rham and G. Gabadadze, Generalization of the Fierz-Pauli action, Phys. Rev. D **82**, 044020 (2010).
[41] C. de Rham, G. Gabadadze, and A. J. Tolley, Resummation of Massive Gravity, Phys. Rev. Lett. **106**, 231101 (2011).
[42] K. Aoki, A. De Felice, S. Mukohyama, K. Noui, M. Oliosi, and M. C. Pookkillath, Minimally modified gravity fitting Planck data better than ΛCDM, Eur. Phys. J. C **80**, 708 (2020).
[43] M. C. Pookkillath, A. De Felice, and S. Mukohyama, Baryon physics and tight coupling approximation in Boltzmann codes, Universe **6**, 6 (2019).
[44] A. De Felice and S. Mukohyama, Graviton Mass Might Reduce Tension between Early and Late Time Cosmological Data, Phys. Rev. Lett. **118**, 091104 (2017).
[45] N. Bolis, A. De Felice, and S. Mukohyama, Integrated Sachs-Wolfe-galaxy cross-correlation bounds on the two branches of the minimal theory of massive gravity, Phys. Rev. D **98**, 024010 (2018).
[46] D. Blas, J. Lesgourgues, and T. Tram, The cosmic linear anisotropy solving system (CLASS) II: Approximation schemes, J. Cosmol. Astropart. Phys. 07 (2011) 034.
[47] A. J. Mead, J. A. Peacock, C. Heymans, S. Joudaki, and A. F. Heavens, An accurate halo model for fitting non-linear cosmological power spectra and baryonic feedback models, Mon. Not. R. Astron. Soc. **454**, 1958 (2015).
[48] R. Hagala, A. De Felice, D. F. Mota, and S. Mukohyama, Non-linear dynamics of the minimal theory of massive gravity, Astron. Astrophys. **653**, A148 (2021).
[49] N. Aghanim, Y. Akrami, M. Ashdown, J. Aumont, C. Baccigalupi, M. Ballardini, A. J. Banday, R. B. Barreiro, N. Bartolo *et al.*, Planck2018 results, Astron. Astrophys. **641**, A8 (2020).
[50] B. Sagredo, S. Nesseris, and D. Sapone, Internal robustness of growth rate data, Phys. Rev. D **98**, 083543 (2018).
[51] R. Arjona, J. Garca-Bellido, and S. Nesseris, Cosmological constraints on nonadiabatic dark energy perturbations, Phys. Rev. D **102**, 103526 (2020).
[52] S. Alam, M. Aubert, S. Avila, C. Balland, J. E. Bautista, M. A. Bershady, D. Bizyaev, M. R. Blanton, A. S. Bolton, J. Bovy *et al.*, Completed SDSS-IV extended Baryon Oscillation Spectroscopic Survey: Cosmological implications from two decades of spectroscopic surveys at the Apache Point Observatory, Phys. Rev. D **103**, 083533 (2021).
[53] D. M. Scolnic *et al.*, The complete light-curve sample of spectroscopically confirmed SNe Ia from Pan-STARRS1 and cosmological constraints from the combined Pantheon sample, Astrophys. J. **859**, 101 (2018).

[54] A. Kinkhabwala and M. Kamionkowski, New Constraint on Open Cold-Dark-Matter Models, Phys. Rev. Lett. **82**, 4172 (1999).
[55] F. Giacomello, A. D. Felice, and S. Ansoldi, Bounds from ISW-galaxy cross-correlations on generalized covariant Galileon models, J. Cosmol. Astropart. Phys. 03 (2019) 038.
[56] N. Bolis, A. De Felice, and S. Mukohyama, Integrated Sachs-Wolfe-galaxy cross-correlation bounds on the two branches of the minimal theory of massive gravity, Phys. Rev. D **98**, 024010 (2018).
[57] Y.-S. Song, W. Hu, and I. Sawicki, Large scale structure of $f(r)$ gravity, Phys. Rev. D **75**, 044004 (2007).
[58] B. Stlzner, A. Cuoco, J. Lesgourgues, and M. Bilicki, Updated tomographic analysis of the integrated Sachs-Wolfe effect and implications for dark energy, Phys. Rev. D **97**, 063506 (2018).
[59] B. Audren, J. Lesgourgues, K. Benabed, and S. Prunet, Conservative constraints on early cosmology: An illustration of the Monte Python cosmological parameter inference code, J. Cosmol. Astropart. Phys. 02 (2013) 001.
[60] T. Brinckmann and J. Lesgourgues, MONTEPYTHON 3: Boosted MCMC sampler and other features, Phys. Dark Universe **24**, 100260 (2019).
[61] V. Mossa *et al.*, The baryon density of the Universe from an improved rate of deuterium burning, Nature (London) **587**, 210 (2020).
[62] R. Abbott *et al.* (LIGO Scientific and Virgo Collaborations), Tests of general relativity with binary black holes from the second LIGO-Virgo Gravitational-Wave Transient Catalog, Phys. Rev. D **103**, 122002 (2021).
[63] C. M. Will, Solar system versus gravitational-wave bounds on the graviton mass, Classical Quant. Grav. **35**, 17LT01 (2018).
[64] C. S. S. Brandao and J. C. N. de Araujo, A recipe to probe alternative theories of gravitation vian-body numerical simulations. I. Spiral galaxies, Astrophys. J. **750**, 29 (2012).
[65] M. E. S. Alves, F. C. Carvalho, J. C. N. de Araujo, M. Penna-Lima, and S. D. P. Vitenti, Cosmological constant constraints from observation-derived energy condition bounds and their application to bimetric massive gravity, Eur. Phys. J. C **78**, 710 (2018).
[66] L. Shao, N. Wex, and S.-Y. Zhou, New graviton mass bound from binary pulsars, Phys. Rev. D **102**, 024069 (2020).
[67] S. Dubovsky, R. Flauger, A. Starobinsky, and I. Tkachev, Signatures of a graviton mass in the cosmic microwave background, Phys. Rev. D **81**, 023523 (2010).
[68] S. Choudhury, Probing large distance higher dimensional gravity from lensing data, Astropart. Phys. **21**, 559 (2004).
[69] G. Dvali, A. Gruzinov, and M. Zaldarriaga, The accelerated universe and the moon, Phys. Rev. D **68**, 024012 (2003).
[70] C. de Rham, J. T. Deskins, A. J. Tolley, and S.-Y. Zhou, Graviton mass bounds, Rev. Mod. Phys. **89**, 025004 (2017).
[71] T. M. C. Abbott *et al.* (DES Collaboration), Dark Energy Survey year 3 results: Cosmological constraints from galaxy clustering and weak lensing, arXiv:2105.13549.
[72] D. Collaboration, Dark Energy Survey year 3 results: Cosmology from cosmic shear and robustness to data calibration, arXiv:2105.13543.
[73] M. Asgari, C.-A. Lin, B. Joachimi, B. Giblin, C. Heymans, H. Hildebrandt, A. Kannawadi, B. Stlzner, T. Trster, J. L. van den Busch *et al.*, Kids-1000 cosmology: Cosmic shear constraints and comparison between two point statistics, Astron. Astrophys. **645**, A104 (2021).